Flat acoustic sources with frequency response correction based on feedback and feed-forward distributed control

Jen-Hsuan Ho[a)]
Section of Applied Mechanics, Faculty of Engineering Technology, University of Twente, P.O. Box 217, 7500 AE Enschede, The Netherlands

Arthur P. Berkhoff
TNO Technical Sciences, Acoustics and Sonar, P.O. Box 96864, 2509 JG Den Haag, The Netherlands

(Received 21 May 2014; revised 3 February 2015; accepted 22 February 2015)

This paper presents an acoustic source with a small thickness and high bending stiffness. The high bending stiffness is obtained with a sandwich structure in which the face of the sandwich structure internal to the source is perforated to increase the acoustic compliance, thereby leading to increased electroacoustic conversion efficiency. Multiple actuators are used to drive the moving component of the acoustic source. Control of the acoustic resonances and structural resonances is required to obtain an even frequency response. The use of collocated decentralized feedback control based on velocity sensing was found to be ineffective for controlling these resonances due to the destabilizing asymmetric modes caused by the coupling of the internal acoustic cavity and the rigid body vibration of the moving component. Resonances can be controlled by a set of independent combinations of symmetric driving patterns with corresponding velocity feedback controllers such that the fundamental mass-air resonance is effectively controlled, as is the lowest bending mode of the moving component. Finally, a compensation scheme for low frequencies is used which enables a flat frequency response in the range of 30 Hz to 1 kHz with deviations smaller than 3 dB.
 [http://dx.doi.org/10.1121/1.4914997]

[MRB] Pages: 2080–2088

I. INTRODUCTION

Acoustic sources having small thicknesses offer practical advantages for active noise control[1,2] and for audio reproduction[3] because the available space is often limited. The electroacoustic efficiency of a moving coil loudspeaker at low frequencies is proportional to the internal enclosure volume.[4,5] Therefore, the available internal volume of the loudspeaker should be used as efficiently as possible. Furthermore, conventional moving-coil loudspeakers attempt to move the membrane or panel as a rigid piston.[4] However, in reality, the membrane exhibits bending waves. These unwanted bending modes of the membrane cause the frequency response of the loudspeaker to be colored and uneven. To achieve an even frequency response, many researchers have designed materials, structure, and suspension for the membrane to eliminate these unwanted resonances. Instead of eliminating these unwanted bending modes, the distributed mode loudspeakers (DML) technique uses these bending modes to produce an acoustic output.[6,7] The excitation position is designed to produce an evenly distributed modal density, which produces an effect similar to a continuous spectrum. Various filter topologies have been studied to further equalize uneven frequency responses. The DML technique offers the advantages of compactness and omnidirectionality. However, the panel resonances are complex and difficult to control, which often leads to complicated computations and an insufficient low-frequency response. In a further development of DMLs, multiple exciters are applied to the panel in a technique known as a multi-actuator panel (MAP).[8,9] However, the panel response is dependent on the excitation positions. Therefore, dedicated filters based on the excitation positions for each individual exciter are essential,[10] although commercial DML products have been seen on the market, and further applications of MAPs have been proposed. For instance, MAPs can function as array loudspeakers for wave field synthesis applications.[8] However, DMLs and MAPs continue to suffer from poor acoustic responses at low frequencies. In a recent study, the bandwidth of a MAP loudspeaker was extended down to 100 Hz by a physical-psychoacoustic combined method.[11] Furthermore, air cavities between two panels are often used to improve noise insulation by passive means.[12–14] A larger air gap provides larger acoustic compliance, and therefore, less coupling is obtained. Compact partitions with narrow air gaps lead to less acoustic insulation, especially at low frequencies. Nevertheless, if a flat acoustic source with small thickness and sufficient acoustic output at low frequencies is provided, the acoustic insulation at low frequencies can be improved by applying an acoustic source for active noise control, while sufficient insulation at high frequencies is provided by a narrow air gap.

In this study, a honeycomb sandwich structure is used as the sound radiation panel because this structure has a low density and high bending stiffness. These properties lead to a low modal density. The low modal density reduces the complexity of the panel vibration, which provides more stable control if the panel is controlled at low frequencies. Furthermore, the honeycomb sandwich structure is combined with a thin cavity, and the face of the sandwich structure

[a)]Author to whom correspondence should be addressed. Electronic mail: j.ho@utwente.nl

internal to the source is perforated to increase the acoustic compliance and the electroacoustic conversion efficiency.[15] The perforated honeycomb panel structure, which is the moving component of the acoustic source, is driven by multiple actuators. To obtain an even frequency response, distributed direct velocity feedback control is applied to control the acoustic and structural resonances. However, the collocated decentralized feedback control can destabilize asymmetric modes caused by the coupling of the internal acoustic cavity and rigid body vibration of the moving panel, but a properly designed sensor-actuator configuration can effectively control these resonances. Moreover, the response of the acoustic source can potentially be improved by equalizing both the magnitude and phase response with digital filters.[16–18] For instance, an inner-outer factorization can determine a minimum-phase transfer function with a stable inverse, which can be used to equalize the frequency response.[19] Based on the inner-outer factorization, a minimum-phase regularized inverse (MPRI) method is used to obtained the optimum frequency response equalization with limited inverse gain.[20,21] An approximate method is the Linkwitz filter, which is a simple method of compensating the response at low frequencies.[22] A comparison between the MPRI method and the Linkwitz filter is given. The principal contributions of the present work are (1) the use of a perforated honeycomb panel as the radiating panel in a thin acoustic source; (2) the distributed feedback control combined with feed-forward control applied to this panel; and (3) the detailed control stability analysis and the provided sensor-actuator configuration design principles.

This paper has four main sections. Section II describes a perforated honeycomb panel structure combined with a cavity, a multichannel decentralized feedback control system for a fully coupled plant matrix, a method for control stability analysis, and methods for compensating insufficient responses at low frequencies. Section III describes the implementation and the experimental setup. Section IV presents the stability analysis of the system, where the excitation positions and a Nyquist analysis are studied. Various control configurations are discussed in Sec. V. The control performance, in terms of the measured sound pressure level (SPL) response above the flat panel loudspeaker, is presented, and the control principles are discussed.

II. METHOD

A. Perforated honeycomb panel

The modal complexity of a panel should be minimized to allow the panel to be controlled with a relatively simple control system. Therefore, a honeycomb sandwich structure, which provides high stiffness and low density, is used as the sound-radiating panel. Moreover, the honeycomb sandwich structure includes one perforated panel, which is connected to a cavity. Thus, the air inside the honeycomb structure can flow in and out of the cavity through the holes in the perforated panel. In other words, the total effective air volume is both the air inside the cavity and the air inside the honeycomb structure. Therefore, the effective air layer thickness is increased, and the dimensions of the cavity can be reduced.

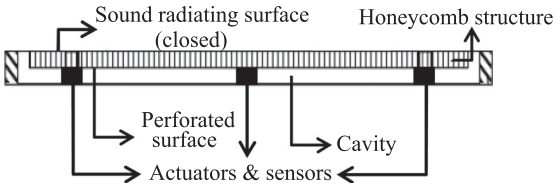

FIG. 1. Side view of the flat panel loudspeaker configuration.

Figure 1 presents the configuration of the flat panel loudspeaker. Actuators and sensors can be applied to drive and to control the panel providing an active controlled flat panel loudspeaker.

Moreover, the radius of the holes, the distance between the holes, and the area ratio of the holes to the perforated panel are considered to guarantee that the air can flow in and out through the perforated panel with a negligible viscous effect. A lumped-element acoustic model of the perforated panel coupled with the cavity and actuators is constructed to verify if the acoustic impedance of the perforated panel is negligible compared to the cavity and honeycomb panel. The acoustic impedance of a circular hole in a plate can be approximated by the acoustic impedance of a non-moving short tube. The acoustic impedance Z_{perf} [N s m^{-3}] of the perforated plate is modeled based on Beranek's approximate model,[23]

$$Z_{\text{perf}} = \frac{\rho}{S_p \sigma}\left\{\sqrt{2\eta\omega}\left[\frac{t_p}{r} + 2\left(1 - \frac{\pi r^2}{{d_h}^2}\right)\right] + j\omega\left[t_p + 1.7r\left(1 - \frac{r}{d_h}\right)\right]\right\}, \tag{1}$$

where ρ [kg m^{-3}] is the density of air, S_p [m^2] is the area of the perforated plate, σ is the dimensionless area porosity, η is the dynamic viscosity, ω [rad s^{-1}] is the angular frequency, t_p [m] is the plate thickness, r [m] is the hole radius, d_h [m] is the distance between the holes, and j is the unit imaginary number. The real part of Z_{perf} corresponds to viscous losses. The friction between the air and the plate interface in the hole is considered. The imaginary part of Z_{perf} corresponds to the mass of air moving insides the hole plus a correction to approximate the total effective moving air mass. This model is valid within the frequency range wherein the frequency f [Hz] satisfies

$$\frac{0.01}{\sqrt{f}} \le r \le \frac{10}{f}, \tag{2}$$

which indicates that the hole size is much smaller than the acoustic wavelength. For the perforated panel in this study, the model is be valid between 15 Hz and 4 kHz. Neglecting the radiation impedance, including mass effects, the acoustic impedances of the cavity and the honeycomb plate correspond to the air volume of the cavity and the hollow space of the honeycomb structure, respectively. The volume velocity flowing into the honeycomb plate is equal to the volume velocity through the perforated plate. The difference between the volume velocity of the radiating plate and the volume velocity flowing into the honeycomb plate is equal to the

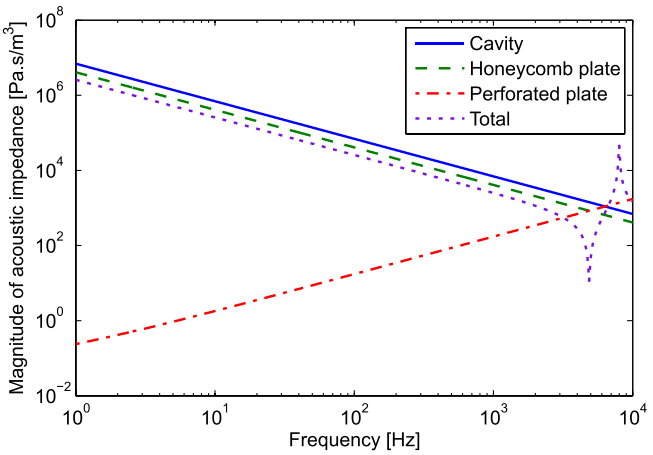

FIG. 2. (Color online) Lumped acoustic impedance load as seen from the back of the radiating structure.

volume velocity flowing into the cavity. Therefore, the total acoustic impedance loading the flat panel is given by

$$Z_{\text{total}} = \frac{1}{\frac{1}{Z_{\text{cav}}} + \frac{1}{Z_{\text{perf}} + Z_{\text{hon}}}}, \tag{3}$$

where Z_{total} [N s m^{-3}] is the total acoustic impedance of the flat panel loudspeaker, Z_{cav} [N s m^{-3}], Z_{perf} [N s m^{-3}], and Z_{hon} [N s m^{-3}] are the acoustic impedance of the cavity, the perforated plate, and the honeycomb plate, respectively. The acoustic impedance frequency responses of the perforated panel, honeycomb panel, and cavity are shown in Fig. 2. The acoustic impedance of the perforated panel is negligible compared to the cavity and honeycomb panel below 1 kHz. Furthermore, a validated structural-acoustic coupled finite element method (FEM) model,[24,25] which can accurately predict the resonance frequencies and mode shapes of the system, has been developed and is used in our work.

B. Multiple decentralized feedback control

To improve the uneven frequency response of the panel, we apply a direct velocity feedback control to the panel. This direct velocity feedback control functions as active damping on the panel to flatten the peaks and dips of the response. Then, the feedback control signal is combined with the driving signal of the loudspeaker to compensate the colored response. Figure 3 illustrates the signal block diagram of a feedback control system. $\mathbf{e}(j\omega)$ is the error signal matrix, where ω is the angular frequency [rad s^{-1}] and $j = \sqrt{-1}$. $\mathbf{G}(j\omega)$ is the plant transfer matrix; $\mathbf{u}(j\omega)$ is the feedback control signal matrix; $\mathbf{d}_d(j\omega)$ is the original driving source matrix, which is the error signal without the input feedback control signal; and $\mathbf{H}(j\omega)$ is the control matrix, which is a constant in the current work. The time-dependent signals are the real part of the complex vectors [i.e., the time-dependent error signal $\mathbf{e}(t) = \text{Re}\{\mathbf{e}(j\omega)e^{j\omega t}\}$]. From the block diagram in Fig. 3, $\mathbf{e}(j\omega)$ can be derived as

$$\mathbf{e}(j\omega) = [\mathbf{I} + \mathbf{G}(j\omega)\mathbf{H}(j\omega)]^{-1}\mathbf{d}_d(j\omega)\mathbf{G}(j\omega), \tag{4}$$

where $\mathbf{I}$ is an identity matrix. To present the physical interactions between each control unit in a multiple-input, multiple-output (MIMO) control system, a fully coupled multiple channel plant transfer matrix $\mathbf{G}(j\omega)$ is applied:

$$\mathbf{G}(j\omega) = \begin{bmatrix} \mathbf{G}_{11}(j\omega) & \cdots & \mathbf{G}_{1m}(j\omega) \\ \vdots & \ddots & \vdots \\ \mathbf{G}_{l1}(j\omega) & \cdots & \mathbf{G}_{lm}(j\omega) \end{bmatrix}, \tag{5}$$

where $\mathbf{G}_{lm}(j\omega)$ is the transfer matrix from the mth actuator to the lth sensor.

In theory, the stability of a feedback control system can be unconditionally guaranteed when the sensors and actuators are dual and collocated.[26] However, practical applications can involve non-ideal conditions. For a single-input, single-output (SISO) control system, the Nyquist stability criterion is used to determine the stability of the system. The system is stable if and only if the locus of $\mathbf{G}(j\omega)\mathbf{H}(j\omega)$ does not cross or encircle $(-1, 0)$. To determine the stability of a MIMO control system, the generalized Nyquist stability criterion is applied. The system is stable if and only if the locus of $\det[\mathbf{I} + \mathbf{G}(j\omega)\mathbf{H}(j\omega)]$ does not cross or encircle the origin $(0, 0)$.[27]

The configuration of actuators and sensors used in the current work is shown in Fig. 4. Five actuators and five sensors are applied to the panel to drive and to control the flat panel loudspeaker. These actuators and sensors are placed collocated. Actuators/sensors 1–4, which are referred to as the corner actuators/sensors, are placed in the corner of the panel, and actuator/sensor 5, which is referred to as the center actuator/sensor, is placed in the center of the panel. Various SISO and MIMO control configurations are studied. In this study, the MIMO control configuration refers to a multiple SISO control configuration. Two cases of a SISO feedback control system are analyzed. In the first case,

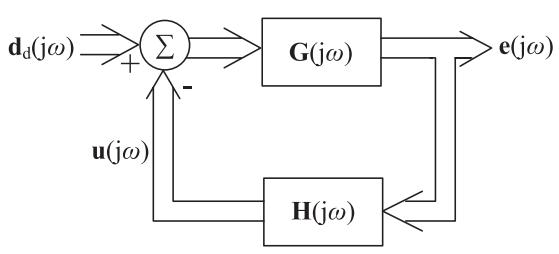

FIG. 3. Feedback control systems.

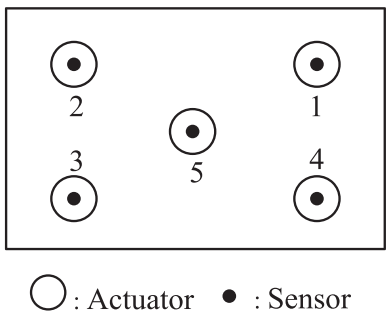

FIG. 4. The configuration of actuators and sensors on the flat panel.

referred to as SISO control with center sensor, the error signal is measured by the center sensor, and the same control signal is sent to all five actuators. In the second case, referred to as SISO control with corner sensor, one of the corner sensors is used as the error sensor, and the five actuators are driven by the same control signal. Furthermore, three cases of the distributed MIMO control system are presented. In the first case, referred to as five-channel MIMO control, all five sensors are used, and the control signal is fed back individually to the collocated actuators. In the second case, referred to as two-channel MIMO control, one center sensor is operating as the error sensor of the center actuator and one corner sensor is operating as the error sensor of the four corner actuators. In the third case, referred to as three-channel MIMO control, three sensors are applied: (1) the center sensor as the error sensor of the center actuator; (2) corner sensor 1 as the error sensor of the corner actuators 1 and 3, which receive the same control signal; (3) corner sensor 2 as the error sensor of the corner actuators 2 and 4, which receive the same control signal. The analysis of these SISO and MIMO control systems is presented in Secs. IV and V.

C. Feed-forward response correction filter

To equalize the response of the loudspeaker at low frequencies, a minimum-phase regularized inverse (MPRI) method is used.[19–21] Inverse filtering methods for equalizing a loudspeaker are based on the concept that one can inverse the filtering caused by the loudspeaker. An inverse filter is designed based on the measured response of the loudspeaker, such that applying the inverse filter to the loudspeaker system results in an uncolored frequency response. However, there is not a guaranteed inverse transfer function for every system. Therefore, the MPRI method applies an inner-outer factorization technique to determine a minimum-phase transfer function, which has a guaranteed stable inverse. This inverse is used to equalize the frequency response of the loudspeaker. Furthermore, if there is a large dip in the frequency response of the loudspeaker, the inverse filter would have a large gain which may cause overloading of the system. Therefore, the MPRI method applies a regularized gain to limit the maximum gain of the inverse filter avoiding an overloading system.

The inverse is based on an $L \times M$-dimensional transfer function $\mathbf{G}(q)$ obtained from system identification,[28] in which q is the unit delay operator. An identified state-space model is augmented with a regularizing function $\mathbf{G}_{\text{reg}}(q)$, which limits the gain of the inverse at frequencies for which the magnitude of $\mathbf{G}(q)$ is small. The augmented state-space model is defined by

$$\bar{\mathbf{G}}(q) = \begin{bmatrix} \mathbf{G}(q) \\ \mathbf{G}_{\text{reg}}(q) \end{bmatrix}. \tag{6}$$

An inner-outer factorization of the augmented state-space model,

$$\bar{\mathbf{G}}(q) = \bar{\mathbf{G}}_i(q)\bar{\mathbf{G}}_o(q), \tag{7}$$

is used to determine an $M \times M$-dimensional minimum-phase transfer function having a stable inverse, for which $\bar{\mathbf{G}}_o^{-1}(q)\bar{\mathbf{G}}_o(q) = \mathbf{I}_L$, in which $\mathbf{I}_L$ is the identity matrix of dimension L. The $L \times M$-dimensional transfer function $\bar{\mathbf{G}}_i(q)$ is an all-pass transfer function, i.e., $\bar{\mathbf{G}}_i^*(q)\bar{\mathbf{G}}_i(q) = \mathbf{I}_M$, in which the asterisk denotes the adjoint operator $\bar{\mathbf{G}}_i^*(q) = \bar{\mathbf{G}}_i^T(q^{-1})$, where T denotes the transpose and $\mathbf{I}_M$ is the identity matrix of dimension M. The all-pass property can be used to show that $\bar{\mathbf{G}}_o^*(q)\bar{\mathbf{G}}_o(q) = \bar{\mathbf{G}}^*(q)\bar{\mathbf{G}}(q) = \mathbf{G}^*(q)\mathbf{G}(q) + \mathbf{G}_{\text{reg}}^*(q)\mathbf{G}_{\text{reg}}(q)$. The inverse is used as the minimum-phase feed-forward response correction filter.

An approximate method that can be used to increase the response of the loudspeaker at low frequencies is to apply a Linkwitz filter as the feed-forward response correction filter. The transfer function of the Linkwitz filter is obtained by dividing the second-order transfer function of the desired loudspeaker,

$$\mathbf{G}_u(s) = \frac{s^2T_u^2}{S^2T_u^2 + \frac{sT_u}{Q_u} + 1}, \tag{8}$$

by that of the second-order uncompensated loudspeaker,

$$\mathbf{G}_d(s) = \frac{s^2T_d^2}{s^2T_d^2 + \frac{sT_d}{Q_d} + 1}, \tag{9}$$

leading to the second-order feed-forward correction filter, the Linkwitz filter,

$$\mathbf{L}(s) = \frac{\mathbf{G}_d}{\mathbf{G}_u} = \frac{s^2T_u^2T_d^2 + \frac{sT_uT_d^2}{Q_u} + T_d^2}{s^2T_u^2T_d^2 + \frac{sT_u^2T_d}{Q_d} + T_u^2}, \tag{10}$$

where s is the Laplace transform parameter. T_u, Q_u, T_d, and Q_d are the coefficients related to the properties of the loudspeaker.

III. IMPLEMENTATION AND EXPERIMENTAL SETUP

We used a 0.5-mm-thick aluminum panel as the closed upper layer of the honeycomb sandwich structure. The perforated lower layer was a 0.3-mm-thick perforated steel panel with holes 5 mm in diameter. These two panels were connected by an aluminum honeycomb structure. The honeycomb sandwich panel had a volume of $605 \times 415 \times 22\,\text{mm}^3$ and a weight of 1.112 kg. The lower perforated panel was attached to a cavity with a depth of 13 mm. The perforated honeycomb panel was suspended by ethylene propylene diene monomer (EPDM) rubber with a thickness of 1 mm and a width of 15 mm. Five voice coil actuators (BEI Kimco Magnetics, type: LA18-12-000A) were mounted on the lower layer of the perforated honeycomb panel. The back view of the at panel loudspeaker is shown in Fig. 5. Each actuator provides a peak force of 44.5 N and a maximum stroke of 3 mm on both sides. The direct current (dc) resistance and the force sensitivity of the actuator are 2.6 Ω and 7.78 N/A.[29]

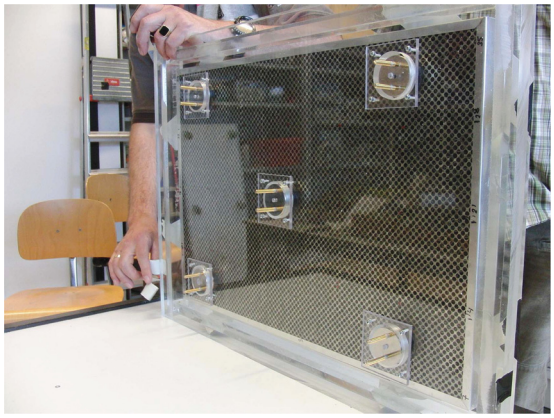

FIG. 5. (Color online) Back view of the flat panel loudspeaker.

Five accelerometers (B&K, type: 4517–002), which functioned as the error sensors for the direct velocity feedback control, were mounted to the upper layer and collocated with the voice coil actuators. The real-time control platform was realized on a field-programmable gate array with a sampling frequency of 100 kHz. Furthermore, an amplifier that delivers a proportional output current based on an input voltage at a constant ratio of 2 A/V was applied to provide the driving current for the voice coil actuators. The near-field sound pressure was measured at 5 cm above the panel.

IV. CONTROL STABILITY

The vibration and sound radiation response of the flat panel greatly depend on the excitation positions. A properly designed excitation position can reduce the complexity of the response. A less complex control system can provide a more stable and simpler feedback control condition. Therefore, we compare the panel response of various excitation positions to determine the excitation configuration. Moreover, a well-designed sensor-actuator configuration can increase the control stability in the feedback control system. Next, another stability analysis is presented. We use the Nyquist criterion to determine and present the control stability of our system. Three sensor-actuator configurations, two SISO control systems, and one distributed MIMO control system, are presented. The frequency range of the analysis is 10 Hz to 1 kHz, which is the range wherein the benefit of this flat panel loudspeaker is expected.

A. Excitation positions

Voice coil actuators were used to excite the panel. The positions of the actuators affect the vibration response of the flat loudspeaker system. The energy of the near-field sound pressure wave is related to the kinetic energy of the radiating panel at lower modes.[30] Therefore, the kinetic energy of the radiating panel can be used to represent the near-field sound. In this section, we used the kinetic energy response of the panel to analyze the effect of the excitation positions. The measured radiated sound pressure response of the panel is presented in Sec. V.

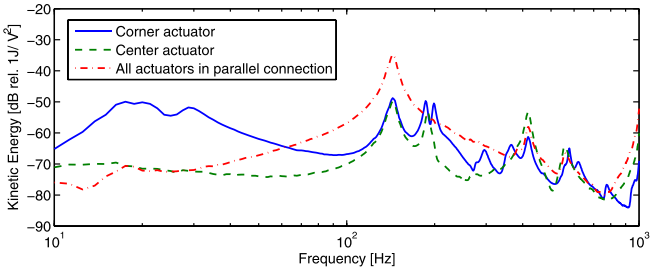

FIG. 6. (Color online) Measured kinetic energy response of the panel with various excitation positions.

The first configuration, wherein we applied one actuator located in the corner of the panel (actuator 1 in Fig. 4), provided an asymmetric excitation force. The second configuration, wherein we applied one actuator located in the center of the panel (actuator 5 in Fig. 4), provided a symmetric excitation force. The third configuration, wherein we applied five equally distributed actuators on the panel in parallel connection, provided a symmetric and equally distributed excitation force. Figure 6 presents the variations in the measured kinetic energy response of the panel for varying excitation positions. The corner actuator, which is located asymmetrically to the panel, excited numerous resonant modes of the system and produced a high modal density. However, a symmetrically located actuator, for example, the center actuator, excited fewer resonant modes than an asymmetrically located actuator. Moreover, applying an equally distributed excitation force, as in the all-actuator configuration, can further reduce the modal density. A less complex panel vibration can provide a more stable and simpler feedback control condition. Therefore, the system design should avoid asymmetric excitation positions. The results have been predicted by a FEM model, and the same conclusions have been given.[24,25]

B. Nyquist stability analysis

The results from the previous section illustrate that driving all actuators with the same signal excites fewer resonant modes; in other words, a single-output control system with

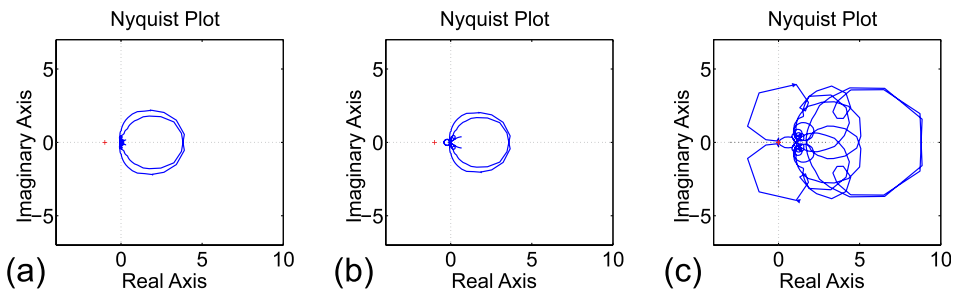

FIG. 7. (Color online) Nyquist plots. (a) SISO with corner sensor, (b) SISO with center sensor, (c) five-channel MIMO control.

TABLE I. Crossover frequency analysis.

	SISO with corner sensor	SISO with center sensor	Five-channel MIMO
Gain crossover frequency [Hz]	28	417	15
Phase crossover frequency [Hz]	129	129	15

an equally distributed force produces a less complex system. However, a distributed control system with multiple controllers provides better controllability and can be applied to a large-scale system without a complicated control loop. Moreover, multiple distributed controllers exhibit a better failure tolerance in the sense that the failure of one controller does not directly affect other controllers. Therefore, in this section, we use the Nyquist criterion and the generalized Nyquist criterion to determine the stabilities of the SISO and MIMO control systems. Two cases of the SISO feedback control and one distributed MIMO control are discussed in this section. The configurations of actuators and sensors of these control systems are introduced in Sec. II B.

The Nyquist plots of these three cases with the same control gain are shown in Fig. 7, and the crossover frequencies are given in Table I. From the Nyquist plots of these three configurations, both of the SISO control systems provide better stabilities than the five-channel MIMO control system. Furthermore, the crossover frequency of the five-channel MIMO control system occurs at 15 Hz with a small control gain. However, the response is more stable, except for the first resonant mode. This result agrees with the previous section. The system resonance at 15 Hz is effectively excited when driving the corner actuator. The distributed five-channel MIMO control system drives these five actuators independently. Using non-identical driving forces yields the same effect as driving at the corner position only. Therefore, this type of excitation force should be avoided.

V. CONTROL RESULTS

In this section, the near-field SPLs measured at 5 cm above the flat panel loudspeaker resulting from various control configurations are presented. First, two configurations of the SISO feedback control system are presented. Then, a designed configuration of the MIMO control system, which can further improve the performance, is presented. Furthermore, the principles of sensor-actuator configuration design are provided. Another MIMO control configuration is presented as an example to demonstrate these principles. Finally, the feedback controller is combined with a feed-forward controller to improve the response of the flat loudspeaker at low frequencies. The detailed experimental setup of the measurements is given in Sec. III.

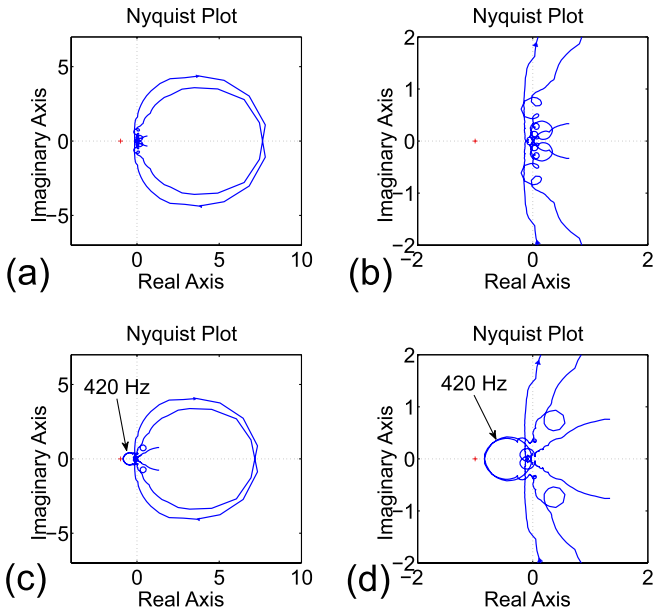

FIG. 8. (Color online) Two SISO control configurations and the Nyquist plot of $\mathbf{G}(j\omega)\mathbf{H}(j\omega)$ from 10 Hz to 1 kHz. (a) Corner sensor control, (b) zoomed in on $(-1, 0)$ of the corner sensor control, (c) center sensor control, (d) zoomed in on $(-1, 0)$ of the center sensor control.

A. Feedback control configurations

1. SISO control system

Section IV illustrates that SISO control provides more stability than five-channel MIMO control in our system. Therefore, we began with SISO control. We only used one sensor to obtain the error signal and then applied an identical control signal to all five voice coil actuators. Two sensor positions were analyzed; one configuration used one of the corner sensors as the error sensor, and one configuration used the center sensor as the error sensor. Because the accelerometer and voice coil actuator were neither dual nor collocated, the feedback control loop was only conditionally stable. The stability can be guaranteed when the Nyquist plot of $\mathbf{G}(j\omega)\mathbf{H}(j\omega)$ does not cross or encircle $(-1, 0)$. The

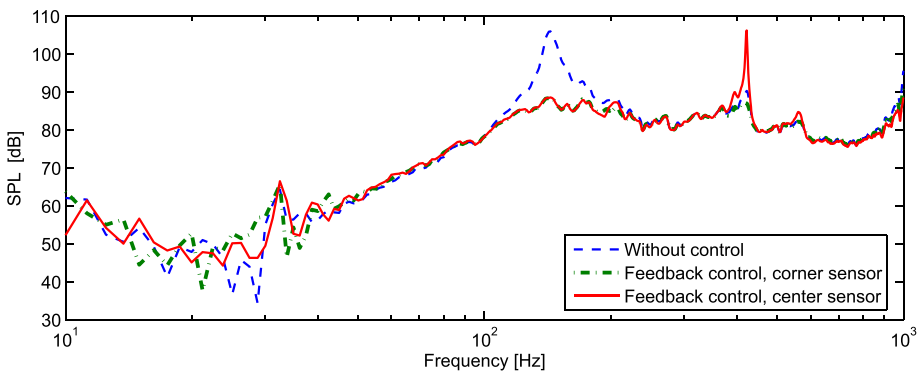

FIG. 9. (Color online) Measured SPL response of the flat loudspeaker with a SISO feedback control.

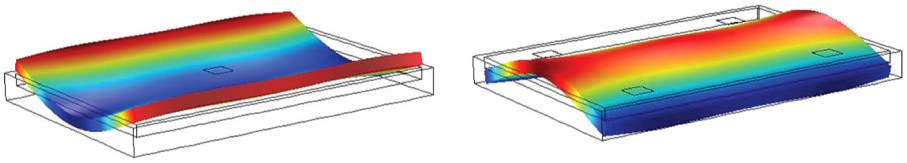

FIG. 10. (Color online) Mode shape at 420 Hz.

Nyquist plots of the system are shown in Fig. 8 and confirm the stability. The feedback controller was realized by using three concatenated infinite impulse response second order filters and a fixed constant control gain for each control channel. First, a low-pass filter was used to integrate the signal from the accelerometer to velocity signal. The cut-off frequency was selected to be at 10 Hz. However, the signal from the accelerometer contained a dc offset which was caused by gravitation. Therefore, a high-pass filter was placed in front of the low-pass filter to prevent saturation of the integrator. The cut-off frequency of this high-pass filter was 5 Hz. Then, the integrated signal, which was the velocity signal, was multiplied by a fixed constant control gain to be used as the control signal. Finally, an additional roll-off low-pass filter with a cut-off frequency at 10 kHz was used to minimize spillover and increase control stability.

The near-field SPL response to the control is shown in Fig. 9. The first resonance peak was greatly reduced by both of the control configurations. However, the resonance peak at 420 Hz was only slightly reduced when using the corner sensor and was actually increased when using the center sensor. This resonance at 420 Hz causes control system instability, as shown in Fig. 8(d). Further sensor-actuator configuration design is necessary to further improve the SPL response.

2. MIMO control system

To improve the control performance at 420 Hz, we further investigated the resonant mode shape at this frequency. Figure 10 presents the mode shape at 420 Hz. The mode shape illustrates that the center point moves opposite to the corner points at this frequency. Therefore, the use of either the center sensor or the corner sensor cannot fully control the vibration of the panel.

Additional sensors are necessary to accurately detect the vibration of the panel. Nevertheless, the figure illustrates that these four corner points move together at this resonance frequency. Therefore, two sensors are sufficient to further improve the control performance at 420 Hz. We applied two sensors, with one center sensor operating as the error sensor of the center actuator and one corner sensor operating as the error sensor of the four corner actuators. The configuration of actuators and sensors is shown in Fig. 4. The generalized Nyquist criterion was applied to confirm the stability of the MIMO control system. The near-field SPL response of the control results is shown in Fig. 11. With this two-channel control, both the first resonance peak and the resonance peak at 420 Hz can be effectively reduced. The result illustrates that all the resonance peaks below 1 kHz can be effectively reduced by this control configuration.

3. Example

A further sensor-actuator analysis based on the previous results is presented in this section. The design follows two principles. First, the excitation positions should be symmetric, and second, the sensor-actuator configuration should consider the fact that the center point moves in the opposite direction of the corner points at the resonance frequency 420 Hz. As an example, a three-channel MIMO control system was measured. The detailed configuration of actuators and sensors are described in Sec. II B. The generalized Nyquist criterion was applied to confirm the stability of the MIMO control system. The near-field SPL response of the three- and two-channel control configurations is shown in Fig. 12. The figure illustrates that the three- and two-channel MIMO control systems exhibited a similar performance.

B. Response equalization at low frequencies

In this section, we applied a feed-forward response correction filter to further improve the insufficient response of the loudspeaker at low frequencies. Three filters, i.e., two MPRI filters and one Linkwitz filter, used to compensate the measured feedback control response are presented in Fig. 13. The first MPRI filter equalized a single pressure response. The plant transfer function was between the driving signal and the near-field sound pressure measured at 5 cm above the loudspeaker. A state-space model of the measured

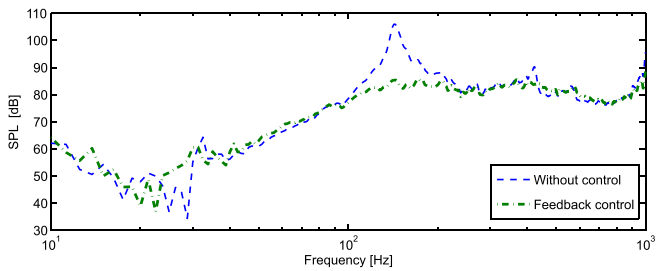

FIG. 11. (Color online) Measured SPL response of the flat loudspeaker with a two-channel MIMO feedback control.

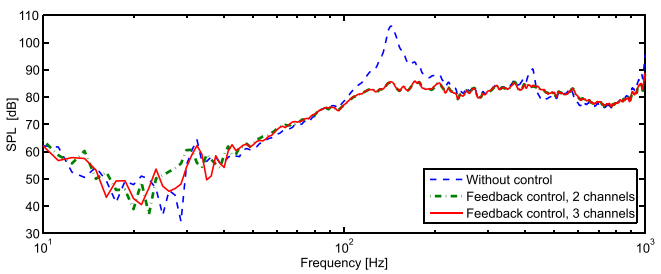

FIG. 12. (Color online) Measured SPL response of the flat loudspeaker with a MIMO feedback control: two-channel configuration (dashed-dotted line) and three-channel configuration (solid line).

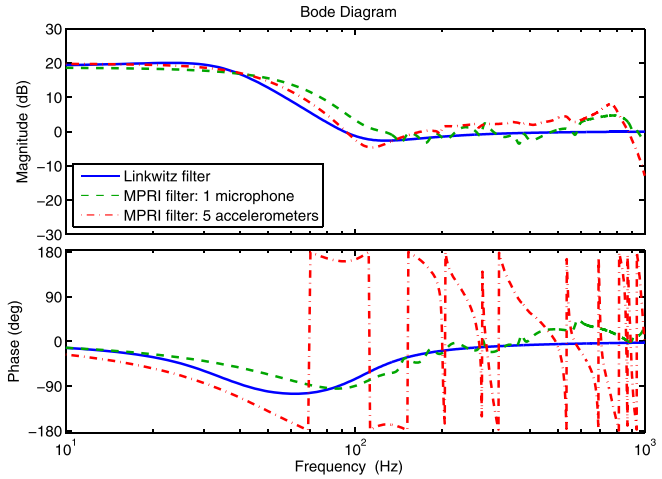

FIG. 13. (Color online) Bode plot of three filters based on measured feedback-controlled response: the Linkwitz filter (solid line), the MPRI filter with one microphone (dashed line), and the MPRI filter with five accelerometers (dashed-dotted line).

transfer function was estimated and was augmented with a regularizing function as shown in Eq. (6). A minimum-phase transfer function, which guaranteed a stable inverse, was determined by applying the inner-outer factorization. The inverse of this minimum-phase transfer function was the first MPRI filter. The second MPRI was obtained by five accelerometers, where the transfer function was between the driving signal and the integrated signal from these five accelerometers. The result indicates there is good potential for the MPRI filter applied in a MIMO control system. The Linkwitz filter design was based on the properties of the feedback controlled panel loudspeaker. The cut-off frequency of the feedback controlled panel loudspeaker was 105 Hz. The target cut-off frequency was selected to be 35 Hz such that the maximum gain of the filter was limited to 20 dB. The second-order Linkwitz filter gives similar compensation to the MPRI filter, which offers an optimum response equalization, as shown in Fig. 14. Therefore, we implemented the second-order Linkwitz filter in the real-time control system. The measured near-field SPL response above the loudspeaker resulting from two- and three-channel distributed feedback and feed-forward combined MIMO control systems is shown in Fig. 15. The response illustrates that with the feed-forward control, the attenuated response of the loudspeaker at low frequencies can be compensated without affecting the feedback control performance.

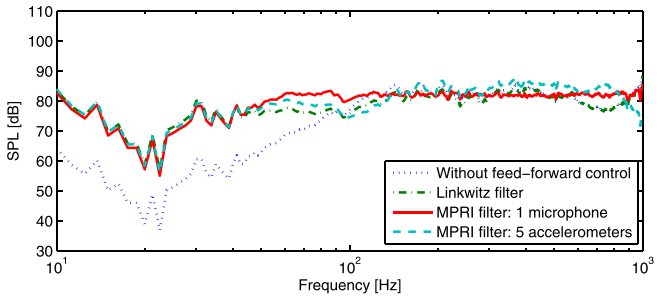

FIG. 14. (Color online) Simulated SPL response equalization based on measured feedback-controlled response: without equalization (dotted line) and with the Linkwitz filter (dotted-dashed line), the MPRI filter with one microphone (solid line), and the MPRI filter with five accelerometers (dashed line).

VI. CONCLUSIONS

This paper presents an acoustic source with a small thickness that provides an even frequency response. Real-time control results indicate that the frequency response of the radiated sound from a perforated honeycomb panel combined with a thin cavity can be improved by applying a simple and stable distributed feedback and feed-forward combined control system to the panel. However, an inappropriate sensor-actuator configuration could easily destabilize the asymmetric resonant modes caused by the coupling of the internal acoustic cavity and the rigid body vibration of the panel. In particular, it was shown that a straightforward decentralized controller based on collocated force actuators and velocity sensors fails to meet the performance requirement because of a destabilizing mode at 15 Hz. The detailed stability analysis in this paper illustrates that more sensor-actuator control channels cannot guarantee the control stability. In contrast, fewer channels can provide a stable control system if the sensor-actuator configuration follows the design principle whereby the excitation force should be symmetrically applied on the panel. A designed set of independent combinations of symmetric driving patterns with corresponding velocity feedback controllers can effectively control both the fundamental mass-air resonance and lower bending modes of the panel. However, the minimum number of sensors depends on the mode shapes within the working bandwidth. The perforated honeycomb panel presented in this work provides a lower modal density. The distributed feedback control system can effectively flatten the frequency response of the perforated honeycomb panel below 1 kHz

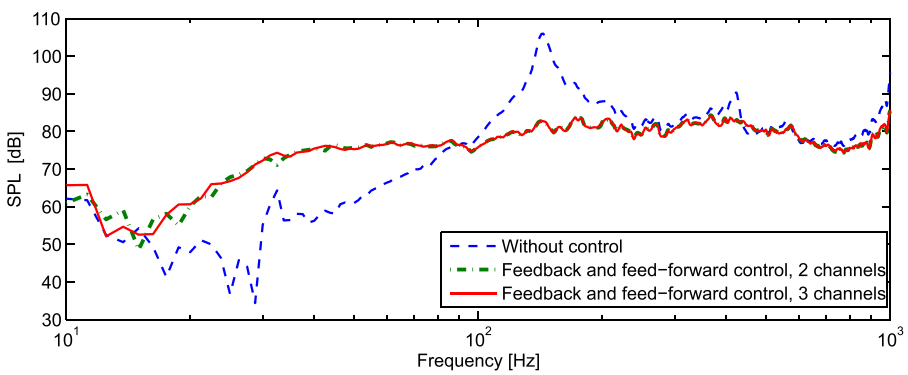

FIG. 15. (Color online) Measured SPL response of the flat loudspeaker with a feedback and feed-forward combined MIMO control system: two-channel configuration (dashed-dotted line) and three-channel configuration (solid line).

with only two accelerometers. Furthermore, the perforated honeycomb panel increases the acoustic compliance and therefore improves the electroacoustic conversion efficiency. Finally, as an example of the compensation scheme for the response at low frequencies, the Linkwitz filter, which provides results similar to the optimum equalization offering by the MPRI filter in this study, is applied as the feed-forward control. A flat frequency response in the range of 30 Hz to 1 kHz with deviations smaller than 3 dB is obtained at a thickness of 35 mm.

ACKNOWLEDGMENTS

This work was supported by STW (De Stichting voor de Technische Wetenschappen, The Foundation for Technical Sciences), Project No. 10602 IMPEDANCE (Integrated Modules for Power Efficient Distributed Active Noise Cancelling Electronics). The experimental development was supported by Henny Kuipers of the Robotics and Mechatronics Group and Geert Jan Laanstra of the Services, Cybersecurity and Safety Group, Faculty of EEMCS, University of Twente.

[1]S. J. Elliott and P. A. Nelson, "Active noise control," IEEE Sign. Process. Mag. **10**, 12–35 (1993).
[2]B. K. Henderson, Steven A. Lane, Joel Gussy, Steve Griffin, and Kevin M. Farinholt, "Development of an acoustic actuator for launch vehicle noise reduction," J. Acoust. Soc. Am. **111**, 174–179 (2002).
[3]W. P. J. de Bruijn and M. M. Boone, "Application of wave field synthesis in life-size videoconferencing," in *Proceedings of the 114th Convention of the Audio Engineering Society*, Delft, The Netherlands (2003).
[4]R. Small, "Direct-radiator loudspeaker system analysis," IEEE Trans. Audio Electroacoust. **19**, 269–281 (1971).
[5]D. Beer, M. Jahr, A. Reich, and M. Schuster, "The air spring effect of flat panel speakers," in *Proceedings of the 124th Convention of the Audio Engineering Society*, Munich, Germany (2008).
[6]N. Harris and M. J. Hawksford, "The distributed-mode loudspeaker (DML) as a broad-band acoustic radiator," in *Proceedings of the 103rd Convention of the Audio Engineering Society*, New York (1997).
[7]N. J. Harris and M. O. J. Hawksford, "Introduction to distributed mode loudspeakers (DML) with first-order behavioural modelling," IEE Proc. Circ. Dev. Syst. **147**, 153–157 (2000).
[8]M. M. Boone, "Multi-actuator panels (MAPs) as loudspeaker arrays for wave field synthesis," J. Audio Eng. Soc. **52**, 712–723 (2004).
[9]M. Kuster, D. De Vries, D. Beer, and S. Brix, "Structural and acoustic analysis of multiactuator panels," J. Audio Eng. Soc. **54**, 1065–1076 (2006).
[10]B. Pueo, J. J. Lpez, G. Ramos, and J. Escolano, "Efficient equalization of multi-exciter distributed mode loudspeakers," Appl. Acoust. **70**, 737–746 (2009).
[11]B. Pueo, G. Ramos, and J. J. Lopez, "Strategies for bass enhancement in multiactuator panels for wave field synthesis," Appl. Acoust. **71**, 722–730 (2010).
[12]S. J. Pietrzko and Q. Mao, "New results in active and passive control of sound transmission through double wall structures," Aerosp. Sci. Technol. **12**, 42–53 (2008).
[13]J. H. Ho and A. Berkhoff, "Comparisons between various cavity and panel noise reduction control methods in double-panel structures," J. Acoust. Soc. Am. **131**, 3501 (2012).
[14]J. H. Ho and A. Berkhoff, "Comparison of various decentralised structural and cavity feedback control strategies for transmitted noise reduction through a double panel structure," J. Sound Vib. **333**, 1857–1873 (2014).
[15]A. P. Berkhoff, "Sound generator, 2010," U.S. patent US20100111351A1 (May 6, 2010).
[16]R. Greenfield and M. J. Hawksford, "Efficient filter design for loudspeaker equalization," J. Audio Eng. Soc. **39**, 739–751 (1991).
[17]M. Karjalainen, E. Piiril, A. Jrvinen, and J. Huopaniemi, "Comparison of loudspeaker equalization methods based on DSP techniques," J. Audio Eng. Soc. **47**, 14–31 (1999).
[18]G. Ramos and J. J. Lpez, "Filter design method for loudspeaker equalization based on IIR parametric filters," J. Audio Eng. Soc. **54**, 1162–1178 (2006).
[19]V. Ionescu and C. Oara, "Spectral and inner-outer factorizations for discrete-time systems," IEEE Trans. Autom. Control **41**, 1840–1845 (1996).
[20]A. P. Berkhoff and G. Nijsse, "A rapidly converging filtered-error algorithm for multichannel active noise control," Int. J. Adapt. Control Sign. Process. **21**, 556–569 (2007).
[21]A. P. Berkhoff, "A technique for improved stability of adaptive feedforward controllers without detailed uncertainty measurements," Smart Mater. Struct. **21**, 064003 (2012).
[22]S. Linkwitz, "A three-enclosure loudspeaker system with active delay and crossover: Part 1, 2, 3," Speaker Builder **80**(2–4), 12–25 (1980).
[23]L. L. Beranek, *Acoustics* (McGraw-Hill, New York, 1954), pp. 138–139.
[24]J. H. Ho and A. Berkhoff, "A low density, high stiffness flat loudspeaker with improved sound frequency response," Proc. Meetings Acoust. **19**, 065082 (2013).
[25]J. H. Ho, "Control sources development for transmitted noise reduction through a double panel structure," Ph.D. thesis, University of Twente, Enschede, The Netherlands (2014).
[26]M. J. Balas, "Direct velocity feedback control of large space structures," J. Guid. Contr. Dyn. **2**, 252–253 (1979).
[27]S. J. Elliott, P. Gardonio, T. C. Sors, and M. J. Brennan, "Active vibroacoustic control with multiple local feedback loops," J. Acoust. Soc. Am. **111**, 908–915 (2002).
[28]L. Ljung, *System Identification Toolbox 7: User's Guide* (The MathWorks, Inc., Natick, 2007).
[29]J. C. Villamil Oostra, "Design and analysis of a flat sound generator," Master's thesis, University of Twente, Enschede, The Netherlands (2012).
[30]M. E. Johnson and S. J. Elliott, "Active control of sound radiation using volume velocity cancellation," J. Acoust. Soc. Am. **98**, 2174–2186 (1995).